

Liquid Bridges in Chemically Structured Slit Pores

Antonio Valencia, Martin Brinkmann, and Reinhard Lipowsky*

Max-Planck-Institut für Kolloid- und Grenzflächenforschung, 14424 Potsdam, Germany

Received December 14, 2000. In Final Form: March 7, 2001

Wetting phenomena are theoretically studied for a slit pore or slab geometry between two structured surfaces which contain stripes of lyophilic surface domains. Two different approaches are used and compared: Monte Carlo simulations of lattice gas models and minimization methods applied to effective interface models. Both types of calculations show that the wetting liquid often attains anvil-like bridges which are not translationally invariant parallel to the surface stripes. As a control parameter such as the liquid volume or the surface separation is changed, these bridges undergo morphological wetting transitions to symmetric or asymmetric channel states.

I. Introduction

It has been recently realized that liquid phases which are in contact with structured surfaces exhibit morphological wetting transitions.^{1–3} So far, these transitions have been primarily studied for the simplest surface geometry consisting of a single planar surface. If such a surface contains striped surface domains which are lyophilic, the wetting liquid forms channels which undergo an abrupt transition to a nonuniform state with a single bulge.²

In this article, we address the question of morphological wetting transitions for a slit pore or slab geometry which consists of two opposite surfaces with striped surface domains. Such a surface geometry has been studied previously using various theoretical methods such as computer simulations,⁴ density functional theories,⁵ and interface models.⁶ However, all previous studies were constrained in one important way: the liquid morphology was assumed to be translationally invariant parallel to the surface stripes. In contrast, in the present study we will allow the wetting liquid between the two surfaces to adjust freely and to adopt states with no translational symmetry. As a result, one then finds *anvil-like* bridges as shown in Figure 1. We show that these anvil-like bridges are *generic* rather than exceptional for all real stripes which have a finite length.

From the experimental point of view, a slab geometry with chemically structured surfaces has been realized, for example, in ref 7 using screen printing technology. In this case, the surface domains were circular and had a size in the millimeter regime. Much smaller domain sizes of the value of 30 nm have been created using the “tip”

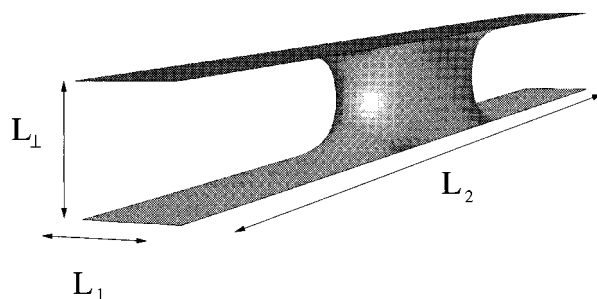


Figure 1. Anvil-like bridge showing long sleeves. The length to width ratio of the lyophilic stripes is $L_2/L_1 = 12$. The ratio of the wall separation to the width of the stripes is $L_1/L_1 = 1.2$. The reduced volume of the liquid is $V/L_1^3 = 4.2$.

of an atomic force microscope, which was brought into contact with another flat surface.⁸ Other methods which could be used, for example, to chemically structure the two opposing surfaces of a surface force apparatus, include elastomer stamps,^{9,10} vapor deposition through grids,¹¹ photolithography of amphiphilic monolayers,¹² lithography with colloid monolayers,¹³ atomic beams modulated by light masks,¹⁴ and microphase separation in diblock copolymer films.¹⁵ If a structured slit pore or slab is prepared by any of these methods, wetting within such a geometry should typically lead to anvil-like bridges as theoretically predicted here.

(1) Lenz, P.; Lipowsky, R. Morphological transitions of wetting layers on structured substrates. *Phys. Rev. Lett.* **1920**, *80*, 1998.

(2) Gau, H.; Herminghaus, S.; Lenz, P.; Lipowsky, R. Liquid morphologies on structured surfaces: from microchannels to microchips. *Science* **1999**, *283*, 46–49.

(3) Lipowsky, R.; Lenz, P.; Swain, P. Wetting and Dewetting of Structured or Imprinted Surfaces. *Colloids Surf., A* **2000**, *61*, 3–22.

(4) Schoen, M.; Diestler, D. J. Liquid vapor coexistence in a chemically heterogeneous slit-nanopore. *Chem. Phys. Lett.* **1997**, *270*, 339–344.

(5) Röcken, P.; Somoza, A.; Tarazona, P.; Findenegg, G. Two-stage capillary condensation in pores with structured walls: A nonlocal density functional study. *J. Chem. Phys.* **1988**, *108*, 8689–8697.

(6) Swain, P. S.; Lipowsky, R. Wetting Between Structured Surfaces: Liquid Bridges and Induced Forces. *Europhys. Lett.* **2000**, *43*, 203–209.

(7) Silver, J.; Mi, Z. H.; Takamoto, K.; Bungay, P.; Brown, J.; Powell, A. Controlled formation of low-volume liquid pillars between plates with a lattice of wetting patches by use of a second immiscible fluid. *J. Colloid Interface Sci.* **1999**, *219*, 81–89.

(8) García, R.; Calleja, M.; Pérez-Murano, F. Local oxidation of silicon surfaces by dynamic force microscopy: Nanofabrication and water bridge formation. *Appl. Phys. Lett.* **1998**, *72*, 2295–2297.

(9) Drelich, J.; Miller, J. D.; Kumar, A.; Whitesides, G. M. Wetting characteristics of liquid drops at heterogeneous surfaces. *Colloids Surf., A* **1994**, *93*, 1–13.

(10) Morhard, F.; Schumacher, J.; Lenzenbach, A.; Wilhelm, T.; Dahint, R.; Grunze, M.; Everhart, D. S. Optical Diffraction – A New Concept for Rapid On-Line Detection of Chemical and Biochemical Analytes. *Electrochem. Soc. Proc.* **1997**, *97*, 1058–1063.

(11) Herminghaus, S.; Fery, A.; Reim, D. Imaging of droplets of aqueous solutions by tapping-mode scanning force microscopy. *Ultra-microscopy* **1997**, *69*, 211–217.

(12) Möller, G.; Harke, M.; Motschmann, H. Controlling microdroplet formation by light. *Langmuir* **1988**, *14*, 4955.

(13) Burmeister, F.; Schäfle, C.; Matthes, T.; Böhmisch, M.; Boneberg, J.; Leiderer, P. Colloid Monolayers as Versatile Lithographic Masks. *Langmuir* **1997**, *13*, 2983–2987.

(14) Drodofsky, U.; Stuhler, J.; Schulze, T.; Drewsen, M.; Brezger, B.; Pfau, T.; Mlynek, J. Hexagonal nanostructures generated by light masks for neutral atoms. *Appl. Phys. B* **1997**, *65*, 755–759.

(15) Heier, J.; Kramer, E. J.; Walheim, S.; Krausch, G. Thin diblock copolymer films on chemically heterogeneous surfaces. *Macromolecules* **1997**, *30*, 6610–6614.

Our article is organized as follows. In section II, the lattice gas models are introduced and details concerning the Monte Carlo simulations are given. In section III, the effective interface models and the numerical minimization methods are presented. The different morphologies of the liquid phase as obtained by both methods are described in section IV. The relation between the chemical potential and the mean curvature of the liquid–vapor interface in the lattice gas model is considered in section V. The shape or “phase” diagram obtained from the numerical minimization of the interface model is presented in section VI. Finally, in section VII our results are compared with those obtained in previous studies that assumed periodic boundary conditions and constant cross section of the liquid morphologies along the stripes.

II. Fluid in a Slit Pore

A. Lattice Gas Model. We study equilibrium liquid morphologies in the slit pore. Each wall of the slit is primarily made of lyophobic material (δ) and contains a lyophilic surface domain (γ) with the shape of a stripe of finite length. Both stripes are identical and face one another on the parallel walls.

Let us consider a lattice gas of particles interacting with nearest neighbors on a simple cubic lattice. The lattice gas is confined to a box with two opposed chemically structured walls and periodic boundary conditions in the directions parallel to these walls. The interaction potential of every particle with the structured walls is short-ranged, and its strength depends on whether the nearest neighbor wall cell belongs to a lyophilic or lyophobic surface domain.

The lattice gas exhibits phase separation at low temperatures, $T < T_C$, and bulk chemical potential $\mu_0 = -3\epsilon$, where the parameter ϵ denotes the interaction strength between two nearest neighbor particles. For the sake of clarity, we will discuss this phase separation in terms of liquid–vapor coexistence. Thus, for $T < T_C$ and $\mu_0 = -3\epsilon$, a high-density liquid phase (β) coexists with a low-density vapor phase (α). In the canonical ensemble, this phase coexistence occurs for intermediate particle number densities ρ with $\rho_\alpha(T) < \rho < \rho_\beta(T)$.

Defining n_i , the occupation number of the i th cell, to be 1 if there is a particle and 0 if there is not, the Hamiltonian of the lattice gas, \mathcal{H}_{LG} , has the form

$$\mathcal{H}_{LG}\{n_i\} = -\epsilon \sum_{\langle ij \rangle} n_i n_j - \sum_{k \in \Omega_1} \epsilon_k n_k \quad (1)$$

where Ω_1 is the set of cells adjacent to the walls. The parameter ϵ is the interaction strength between two nearest neighbor particles, and ϵ_k is the interaction strength of the wall with an adjacent particle. The latter parameter reflects the chemical composition of the wall. The absence of the kinetic energy in \mathcal{H}_{LG} produces a temperature-dependent shift between the chemical potential of the lattice gas, μ , and the chemical potential of the classical fluid, μ_{fluid} , as given by

$$\mu = \mu_{\text{fluid}} + 3k_B T \ln(a/\Lambda_T) \quad (2)$$

where a is the lattice spacing and $\Lambda_T \equiv h/(2\pi m_p k_B T)^{1/2}$ is the thermal de Broglie wavelength. This shift does not affect the differences in chemical potential at a given T , and one has $\mu_{\text{fluid}} - (\mu_0)_{\text{fluid}} = \mu - \mu_0$.

We fix the number of particles in our simulation box (canonical ensemble). In most of our lattice gas simulations, the width L_1 of the stripes is chosen to be 10 lattice units and the length L_2 of the stripes is $12 \times L_1$, see Figure 2. The size of the box in the directions parallel to the

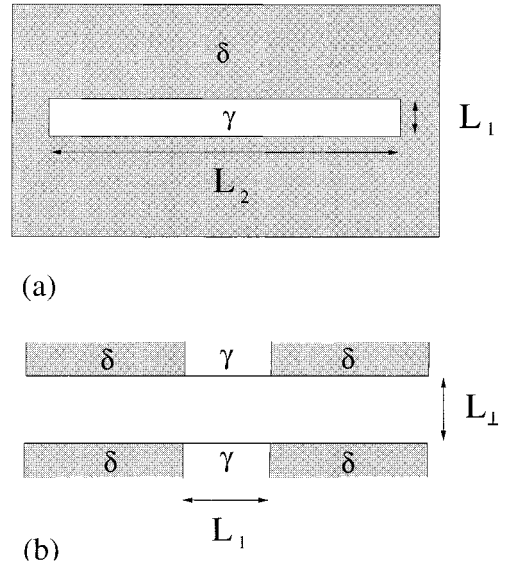


Figure 2. Geometry of the chemically structured slit pore containing lyophilic γ and lyophobic δ surface domains: (a) topview of striped surface domain and (b) sideview of opposing surfaces.

opposed walls is chosen to be large enough so that it does not affect the shape of the dense phase (liquid). In the simulations, the length of the box is set to $13 \times L_1$ and its width to $4 \times L_1$. The separation of the two surfaces varies from $L_\perp = 0.8L_1$ to $L_\perp = 1.6L_1$.

For simplicity, we choose the interaction energy ϵ_γ between the particles and the *lyophilic* surface domains to be equal to the interaction energy between two particles, ϵ , and the *lyophobic* surfaces exert a simple hard core repulsion on the particles. Thus, the interactions between the walls and the particles are given by

$$\epsilon_k = \epsilon_\gamma = \epsilon \text{ and } \epsilon_k = \epsilon_\delta = 0 \quad (3)$$

at the γ and δ surfaces, respectively. The interaction energy $\epsilon_\gamma = \epsilon$ that we choose between the particles and the lyophilic surface domains is the minimum value that leads at any temperature to complete spreading of a homogeneous γ substrate. On the other hand, the coupling $\epsilon_\delta = 0$ that we choose for the lyophobic parts of the walls (only hard core repulsion) is sufficient to induce complete dewetting, that is, contact angle π between the dense phase (liquid) and the δ substrate.

If we map the particles of the lattice gas into spins pointing *up* and the unoccupied cells into spins pointing *down*, the lattice gas is equivalent to an Ising model. First, we show that the lattice gas in the grand canonical ensemble maps into the Ising model in the canonical ensemble. Later, we consider how this mapping is modified for the lattice gas in the canonical ensemble.

We use the change of variables $n_i = (s_i + 1)/2$ in the lattice gas Hamiltonian in (1), so that the variable s_i takes the value $+1$ if the i th cell contains a particle and -1 if the cell contains none. As a result, the combination that enters the grand partition function is now given by

$$\mathcal{H}_{LG}\{s_i\} - \mu N = \mathcal{H}_I\{s_i\} = -J \sum_{\langle ij \rangle} s_i s_j - \sum_{k \in \Omega_1} H_k s_k - H \sum_k s_k + E_0 \quad (4)$$

with

$$J = \frac{\epsilon}{4} \quad H_k = \frac{1}{2} \left(\epsilon_k - \frac{\epsilon}{2} \right) \quad H = \frac{1}{2} (\mu + 3\epsilon) \quad (5)$$

and the constant term

$$E_0 \equiv -\frac{1}{2} \sum_{k \in \Omega_1} \left(\epsilon_k - \frac{\epsilon}{4} \right) - \frac{1}{2} \left(\mu + \frac{3\epsilon}{2} \right) \sum_k$$

\mathcal{H} is the Hamiltonian of the spin- $1/2$ Ising model in an external field H and in contact with walls which exert the surface field H_k onto the adjacent layer of spins. Thus, the grand canonical partition function of the lattice gas, Ξ_{LG} , is proportional to the canonical partition function of the Ising model, \mathcal{Z} , and one has $\Xi_{\text{LG}}(\epsilon, \epsilon_k, \mu) = e^{-E_0/k_B T} \mathcal{Z}(J, H_k, H)$.

From eq 5, the lyophilic areas of the walls, $\epsilon_\gamma = \epsilon$, correspond in the Ising model to surface domains with $H_k = H_\gamma = J$. The lyophobic areas, $\epsilon_\delta = 0$, are characterized by the surface field $H_k = H_\delta = -J$. If the external field is different from zero, $H \neq 0$, the Ising model is in a ferromagnetic state (magnetization per spin, $m \neq 0$) at any finite temperature. If $H = 0$, there is a critical temperature, T_C , so that the Ising model is in a ferromagnetic state ($m \neq 0$) for $T < T_C$ and is in a paramagnetic state ($m = 0$) for $T > T_C$. The case $H = 0$ corresponds to the lattice gas bulk coexistence which, from eq 5, occurs at chemical potential $\mu_0 = -3\epsilon$. At $H = 0$ and $T < T_C$, m has two equilibrium values, $m = \pm m_0(T)$. The particle number density is related to the magnetization per spin via $\rho = (1 + m)/2$. Thus, at $T < T_C$, the lattice gas in the grand canonical ensemble can be found in any superposition of the two states,

$$\rho_+(T) = \frac{1}{2}(1 + |m_0(T)|) \quad \text{and} \quad \rho_-(T) = \frac{1}{2}(1 - |m_0(T)|) \quad (6)$$

where interfacial contributions have been ignored.

For the lattice gas in the canonical ensemble, the same substitution of the occupation numbers, n_i , by the spin variables, s_i , leads to

$$\mathcal{H}_{\text{LG}}\{s_i\} = \mathcal{H}_{\text{I}}\{s_i\} = -J \sum_{\langle ij \rangle} s_i s_j - \sum_{k \in \Omega_1} H_k s_k + E_1 \quad (7)$$

with the constant term

$$E_1 \equiv -3\epsilon N - \frac{1}{2} \sum_{k \in \Omega_1} \left(\epsilon_k - \frac{\epsilon}{4} \right) + \frac{3\epsilon}{4} \sum_k \quad (8)$$

where the parameters J and H_k are again given by eq 5. Thus, in the canonical ensemble, the lattice gas maps into an Ising model in zero external field, $H = 0$, with surface field H_k . The number of states, that the lattice gas in the canonical ensemble can access, is constrained by the conservation of the number of particles, $N = \sum_k n_k$, which translates into the conservation of the total magnetization, $\mathcal{M} = \sum_k s_k = \mathcal{M}(2\rho - 1)$. In the equivalent Ising model, \mathcal{N} stands for the number of cells in the lattice. This implies that the canonical partition function of the lattice gas is given by $\mathcal{Z}_{\text{LG}}(\epsilon, \epsilon_k, N) = e^{-E_1/k_B T} \mathcal{Z}_{\text{I}}(J, H_k, \mathcal{M})$.

If one fixes the density in the lattice gas for $T < T_C$ to a value between the preferred densities of eq 6, the system undergoes phase separation and forms domains with these densities following the lever rule.

The magnetic symmetry $s_k \leftrightarrow -s_k$, $H_k \leftrightarrow -H_k$, and $H \leftrightarrow -H$ maps into the particle-hole symmetry $n_k = 0 \leftrightarrow n_k = 1$, $\epsilon_k - \epsilon/2 \leftrightarrow \epsilon/2 - \epsilon_k$, and $\mu - \mu_0 \leftrightarrow \mu_0 - \mu$. Thus, any phenomena occurring, say, in the vapor phase at $\mu = \mu_0$

$-\Delta\mu$ for the substrate interaction $\epsilon_k = \epsilon/2 - \Delta\epsilon_k$ will have the symmetric image in the liquid phase at $\mu' = \mu_0 + \Delta\mu$ for $\epsilon'_k = \epsilon/2 + \Delta\epsilon_k$. This particle-hole symmetry of the lattice gas makes our results applicable to the *dewetting* of a slit pore with walls which are primarily made of *lyophilic* material and contain two opposing *lyophobic* stripes.

B. Monte Carlo Method. We are interested in studying thermodynamic equilibrium; to reduce relaxation times, we use a nonlocal algorithm, the so-called nonlocal Kawasaki dynamics.¹⁶ A step in this dynamics consists of the following operations. (i) A particle and an unoccupied cell in our simulation box are chosen at random. (ii) The energy change ΔE of moving the selected particle to the selected empty cell is computed from the Hamiltonian in (1). (iii) If ΔE is negative or zero, the move is accepted. If ΔE is positive, the move is accepted with a probability given by $\exp(-\Delta E/T)$, as in the Metropolis scheme. This algorithm leads to relaxation times which are shorter than for the standard (local) Kawasaki method, where the particles can move only to next-neighbor empty cells. In the standard Kawasaki dynamics, the redistribution of the material in the lattice is limited by the time scale needed for the diffusion of the particles. In the nonlocal Kawasaki dynamics, the nonlocal moves allow the particles to redistribute in the lattice without this restriction. However, as far as equilibrium properties are concerned, both dynamics lead to the same sampling of states because both algorithms satisfy detailed balance.

C. Chemical Potential. If the two coexisting phases α and β are sufficiently large, the chemical potential attains its bulk value $\mu_0 = -3\epsilon$ as mentioned. For finite systems as studied here, the substrate surfaces or walls and the $\alpha\beta$ interfaces make a surface contribution to μ and its value will, in general, differ from $\mu_0 = -3\epsilon$. To compute μ in the latter case, we focus on a single lattice site or cell i and treat this cell as a subsystem in chemical equilibrium with the rest of the lattice gas.

The chosen cell interacts with six nearest-neighbor cells, if it is located in the bulk away from the walls, and with five such cells, if it is located directly adjacent to one of the two walls. Each of these nearest-neighbor cells may be empty or occupied by one particle. Now, consider, for a certain cell i , a particular configuration \mathcal{S}_m of m occupied nearest-neighbor cells. For a bulk location, one has $0 \leq m \leq 6$, whereas $0 \leq m \leq 5$ for a surface location. The interaction energy of a particle located in the cell i with the nearest-neighbor configuration \mathcal{S}_m is given by $E(\mathcal{S}_m, n_i) = -m\epsilon n_i$ for a bulk location and by $E(\mathcal{S}_m, n_i) = -(\epsilon_\sigma + m\epsilon)n_i$ for a surface location.

This implies that the chosen cell i can be characterized by the statistical weight or Gibbs factor $f(\mathcal{S}_m, n_i)$ which is proportional to $\exp[-(E(\mathcal{S}_m, n_i) - \mu n_i)/k_B T]$. The probabilities or frequencies $f(\mathcal{S}_m, n_i = 1)$ and $f(\mathcal{S}_m, n_i = 0)$ can be directly measured in the simulations. Following refs 17 and 18, these quantities may then be used in order to determine the chemical potential via

$$\mu/k_B T = \ln[f(\mathcal{S}_m, n_i = 1)/f(\mathcal{S}_m, n_i = 0)] + E(\mathcal{S}_m, n_i = 1)/k_B T \quad (9)$$

To reduce the error in the estimate of the chemical potential, we calculate it as the average of the chemical

(16) Newman, M. E. J.; Barkema, G. T. *Monte Carlo Methods in Statistical Physics*; Oxford University Press: New York, 1999.

(17) Meirovitch, H.; Alexandrowicz, Z. Estimation of the pressure with computer simulation. *Mol. Phys.* **1977**, *34*, 1027–1035.

(18) Binder, K.; Stauffer, D. A simple introduction to Monte Carlo simulation and some specialized topics. *Applications of the Monte Carlo Method in Statistical Physics*. Springer-Verlag: New York, 1987.

potentials obtained for the statistically most significant \mathcal{S}_m configurations.

D. Interfacial Shape. The underlying lattice introduces an anisotropy in the interfacial free energy, giving rise to privileged directions for the drops to have facets. For liquid droplets as considered here, this effect of the lattice is an artifact and can be reduced by fixing a sufficiently high temperature which exceeds the roughening temperature of the interface. In general, the closer the temperature is to the critical temperature, the more isotropic is the interfacial free energy and the larger are the thermal fluctuations. We choose a temperature $T = 0.7 T_C$, where $T_C \approx 1.128 \epsilon / k_B$ is the critical temperature of the three-dimensional bulk lattice gas.¹⁹ This temperature is high enough to reduce the influence of the lattice but still sufficiently far away from the critical temperature so that the interfacial width, which is proportional to the bulk correlation length, is still small.

Away from the interfaces, the particle number density ρ has the values ρ_α and ρ_β in the α and β phases, respectively. In the interfacial region, the density interpolates between these values. We may define the position of the interface as the position of the surface of constant density $\rho_{\alpha\beta}$, with $\rho_\alpha < \rho_{\alpha\beta} < \rho_\beta$. This convention allows us to compare the morphologies of the liquid phase in both models studied here, the lattice gas and the effective interface model.

To find the mean shape of the liquid phase in the lattice gas simulations, one has to average the occupation numbers in every cell for a set of configurations obtained with the previously described algorithm, which determines the probability for each cell to be occupied by a particle. To define a sharp location for the interface, we consider all cells with average density $\rho \leq 0.5$ to be occupied by vapor and all cells with average density $\rho > 0.5$ to be occupied by liquid.

One of the interesting morphologies observed in our simulations is an *anvil-like* bridge with a lateral extension which is small compared to the length of the stripes. Because of the thermal fluctuations, these anvil-like bridges can move along the stripes via diffusion. We want to determine the average shape of one of these bridges. First, we have to obtain the density profile of the bridge, which is the average occupation number for each cell. The diffusional motion of the bridge (which is very slow) is avoided by computing the position of the center of mass at every Monte Carlo step, and if it deviates from the center of the box more than a certain threshold, the configuration is shifted so that the center of mass stays in the center of the box. Finally, we determine the local density by dividing the sum of the occupation numbers at every cell by the number of configurations.

As mentioned, the average shape of the liquid is calculated for a fixed number of particles in the box. Starting with an equilibrium configuration from a former run with a similar number of particles and shifting this number to the new value, we let it relax under nonlocal Kawasaki dynamics for 10^6 Monte Carlo steps. After that time, we perform a long run consisting of 5×10^6 Monte Carlo steps and sample the occupation numbers of the configurations after every 500 steps. Finally, the averages are computed.

III. Fluid–Fluid Interface in a Slit Pore

A. Effective Interface Model. For large systems at temperatures away from the critical point of the fluid, the

effective interface model can be employed to investigate different morphologies of the liquid phase. Because the liquid is essentially incompressible, contributions to the free energy coming from the bulk are neglected and the free energy of our system is equal to the sum of the free energies of all interfaces. In principle, the interface between the vapor and the liquid phase is roughened by capillary waves but this effect is very small and can be safely ignored. We consider the mean interfacial shape which is defined by averaging the position of the interface.

As mentioned before, the vapor and the liquid phase are labeled by Greek letters, α and β , and the lyophilic and the lyophobic regions of the structured walls are designated by γ and δ , respectively. We will focus on wetting structures in the micrometer range for which effects of gravity and line tension are negligibly small and can be neglected. The interfacial free energy per unit area of the liquid–vapor interface, $\Sigma_{\alpha\beta}$, is taken to be independent of the position of the interface as appropriate for an interface between two fluid phases. In contrast, the interfacial free energies per unit area between the substrates and the vapor or liquid phase, $\Sigma_{\alpha\sigma}(\mathbf{x})$ and $\Sigma_{\beta\sigma}(\mathbf{x})$, are functions of the position \mathbf{x} parallel to the surface or walls, σ . The effective free energy of our system, $\tilde{\mathcal{F}}$, depends on the shape and location of the liquid volume, V_β , on the structured walls and is given by

$$\mathcal{F}\{V_\beta\} = \Sigma_{\alpha\beta} |A_{\alpha\beta}| + \int_{A_{\beta\sigma}} dA [\Sigma_{\beta\sigma}(\mathbf{x}) - \Sigma_{\alpha\sigma}(\mathbf{x})] \quad (10)$$

The spatial region occupied by the liquid phase, V_β , is bounded by the interfaces $A_{\alpha\beta}$ and $A_{\beta\sigma}$ toward the vapor phase and the substrate walls, respectively. $|A_{\alpha\beta}|$ denotes the surface area of $A_{\alpha\beta}$. The line of intersection between the two interfaces, $A_{\alpha\beta}$ and $A_{\beta\sigma}$, is the contact line, $\mathcal{L}_{\alpha\beta\sigma}$. $|V_\beta|$ is the volume of the liquid phase for a certain morphology V_β . If the volume of the liquid phase has a constant value, V , the functional

$$\tilde{\mathcal{F}}\{V_\beta\} = \mathcal{F}\{V_\beta\} + \Delta P |V_\beta| \quad (11)$$

has to be minimized in the set of the states satisfying the constraint

$$|V_\beta| = V \quad (12)$$

The parameter ΔP is a Lagrange multiplier and has the physical meaning of the pressure difference, $\Delta P \equiv P_\alpha - P_\beta$, across the liquid–vapor interface. If the volume were not constrained to have a constant value, the last term in (10) would give a nonzero contribution to the free energy.

B. Equilibrium Shapes. The condition of stationarity for the functional in (11) yields two equations which express the mechanical equilibrium of the liquid–vapor interface and the contact line. One is the well-known Laplace equation,

$$\Delta P = -2 \Sigma_{\alpha\beta} M \quad (13)$$

for the pressure difference, $\Delta P \equiv P_\alpha - P_\beta$, which forces the mean curvature, M , to be the same at all points of the liquid–vapor interface. We define the mean curvature, M , in such a way that it has a positive sign for a spherical drop.

The second equation obtained from the first variation of (11) is the Young equation, which ensures the equilibrium of interfacial tensions in the direction parallel to

(19) Pawley, G. S.; Swendsen, R. H.; Wallace, D. J.; Wilson, K. G. Monte Carlo renormalization-group calculations of critical behavior in the simple-cubic Ising model. *Phys. Rev. B* **1984**, *29*, 4030–4040.

the substrate and perpendicular to the contact line at every point \mathbf{x} of the contact line. With the contact angle, $\theta(\mathbf{x})$, measured between the liquid–substrate and the liquid–vapor interface, this equation reads

$$\cos \theta(\mathbf{x}) = \frac{\sum_{\alpha\sigma}(\mathbf{x}) - \sum_{\beta\sigma}(\mathbf{x})}{\sum_{\sigma\beta}} \quad (14)$$

Interfacial shapes satisfying (13) and (14) are stationary but do not have to be minima of the functional in (11) under the constraint in (12). Before we describe the specific interfacial morphologies for the chemically structured slit pore, we first want to discuss two generic properties of these morphologies which can be derived from differential geometry:

(i) *For liquid drops sitting on a single flat substrate, the mean curvature M of the liquid surface has to be positive.* This can be seen by looking at the equilibrium of the forces normal to the substrate at the contact line. Because the component normal to the substrate of the liquid–vapor interfacial tension is always positive along the contact line, the pressure difference across the liquid–vapor interface, $\Delta P \equiv P_\alpha - P_\beta$, has to be negative to compensate this force and keep the liquid surface in equilibrium, and by the Laplace equation M has to be positive. In contrast to this situation, the liquid–vapor interface for a drop sitting between two parallel planar walls can have positive or negative mean curvature depending on the contact angles, volume of liquid, and distance between the walls.

(ii) *The contact line lying within a lyophilic domain with angle $\theta_\gamma = 0$ is always pinned to the $\gamma\delta$ domain boundary for $M > 0$ and may be detached partially or completely from this boundary for $M \leq 0$.* From the Laplace equation, the mean curvature is the same for every point of the liquid surface in equilibrium. Thus, it is sufficient to find its value for a single surface point. At a point of the contact line, \mathbf{x}_0 , lying in the interior of a γ domain with contact angle $\theta_\gamma = 0$, the normal curvature c_1 of the liquid surface in the direction tangential to the contact line has to vanish. The normal curvature c_2 in the direction perpendicular to the contact line at the point \mathbf{x}_0 cannot be positive if the contact angle θ_γ is zero at \mathbf{x}_0 . Because the two normal curvatures correspond to two orthogonal planes of intersection, the mean curvature $M(\mathbf{x}_0)$ is given by $M(\mathbf{x}_0) = (c_1 + c_2)/2$, and we conclude that $M(\mathbf{x}_0) \leq 0$ and that the same inequality must hold for all points of the liquid surface. A more detailed derivation of this statement is given in the Appendix.

C. Slit Pore Geometry. Let us now consider the slit pore geometry described in the foregoing section. We set $\theta_\gamma = 0$ for the lyophilic and $\theta_\delta = \pi$ for the lyophobic domains of the substrate. If the contact line coincides with the boundaries of the lyophilic domains, $\theta(\mathbf{x})$ may assume values between θ_γ and θ_δ .²⁰

The mean curvature of the configurations which minimize the functional in (11) with respect to the volume constraint in (12) depends on the volume of the liquid and the geometry of the slit pore, which is determined by the distance between the walls, L_\perp , the length of the stripes, L_2 , and the width of the stripes, L_1 . It is sufficient to use the ratios L_\perp/L_1 and L_2/L_1 because the free energy in (11) is homogeneous to the second degree if one scales all the lengths of the slit pore. For a given geometry of the slit pore, several minimal configurations, V_β , may exist for a fixed volume V , which form different branches of a

multivalued function $V_\beta(L_\perp, L_2, L_1, V)$. This function has at least one branch and is defined for any volume and geometry of the slit pore, because we must find at least one minimizer of the functional in (11) under the constraint in (12) for every set of parameters. The mean curvature, M , of the configurations belonging to these branches can be displayed as a multivalued function depending on the volume and the geometry of the slit pore, $M(L_\perp, L_2, L_1, V)$.

It may happen that a branch of solutions to the first variational problem of the free energy in (11) under the volume constraint in (12) consists of both stable and unstable regions. The set of configurations dividing these regions must also be part of another unstable branch of solutions.²¹ This corresponds to the occurrence of a soft mode or, equivalently, to the second variation of the functional in (11) becoming positive semidefinite in the subspace of variations which fulfill the volume constraint in (12) to the first order.^{22,23}

D. Minimization Method. We employed the software package Surface Evolver, version 2.14,²⁴ to study the morphologies of a volume of liquid in the slit pore. The surface of the liquid–vapor interface is discretized and replaced by a net of small triangles. To minimize the free energy in (10), we used the implemented conjugate gradient descent method. The volume, that is held constant throughout the minimization, is computed as a surface integral over a vector field with constant divergence on the liquid–vapor surface. The contact lines of the liquid surface are constrained to the walls of the slit pore. Contributions to the free energy coming from the interfaces between the liquid phase and the walls are obtained by line integrals along the contact lines, while the interfacial energy of the liquid–vapor interface is proportional to the area of all triangles forming the surface of the liquid. We measure all interfacial tensions in units of the liquid–vapor interface tension, $\Sigma_{\alpha\beta}$.

Parameters such as the distance L_\perp between the walls, the volume V of the liquid phase, and the contact angles can be varied during the simulation. In most runs, only the volume was changed by a script program, which also maintained the structure of the net forming the liquid surface. It can happen that triangles become very small and collapse after some steps of the minimization procedure. Another typical problem is that long and thin triangles occur whenever large changes in the shape of the configurations take place. Routines which remove undesirable triangles and keep the size of the edges in a certain prescribed range are provided by Surface Evolver and were used every time the volume was changed. Utilizing the query commands of the Surface Evolver script language, we also monitored parameters describing the shape of the configurations such as (i) the diameter of narrow necks within the bridges which form just before they break up or (ii) the positions of some characteristic points of the contact line.

We performed runs for a fixed length and width of the stripes and computed the free energy for 150–300 different values of the volume, depending on the range of volumes

(21) Gillette, R. D.; Dyson, R. C. Stability of fluid interfaces of revolution between equal solid circular plates. *Chem. Eng. J.* **1971**, *2*, 44–54.

(22) Vogel, T. Stability of a liquid drop trapped between two parallel planes. *SIAM J. Appl. Math.* **1987**, *47*, 516–525.

(23) Zhou, L. On stability of a catenoidal liquid bridge. *Pac. J. Math.* **1997**, *178*, 185–198.

(24) Brakke, K. The surface evolver. *Experimental Math. ematics* **1992**, *1*, 141–165.

(20) Lenz, P.; Lipowsky, R. Stability of Droplets and Channels on Homogeneous and Structured Surfaces. *Eur. Phys. J. E* **2000**, *1*, 249–262.

and the shapes of the configurations. Up to 1000 minimization steps were carried out for every value of the volume, depending on the rate of convergence. We took the final configuration obtained for a certain volume as the initial configuration in the minimization procedure for the next volume. If the volume is changed in sufficiently small steps, changes in the configuration are also small, which prevents the configurations from being destabilized by these perturbations, except close to a discontinuous morphological transition. The minimal and maximal length of the edges within the triangulation are adjusted to keep the number of vertexes in the range of 3000–5000 for the liquid surface. If the equilibrium configurations exhibit certain symmetries, a smaller segment of the surface can be employed to compute the interfacial free energy. For example, if the shape has two symmetry planes perpendicular to the walls, one along and the other across the stripes, a segment of the liquid surface consisting of a quarter of the total surface obtained by cuts along the two symmetry planes can be used in the computations. In this reduced model, the boundary of the liquid surface is constrained to move on the symmetry planes with prescribed contact angle $\pi/2$ with respect to these planes, which is equivalent to the mirror boundary conditions.

To save computational time, a quarter of the total liquid–vapor interface was employed in our investigations. One has to be careful with the stability analysis of the bridges, as the number of stationary configurations can be changed because of the constraint imposed by a symmetry. An example of this behavior is the instability of a liquid bridge with its contact line attached to a pair of parallel and coaxial circles. The breaking of the liquid interface is reported to be caused by an asymmetric mode, if the ratio distance between the walls to diameter of the circles is larger than 2.13.²⁵ In the slit pore, a further reduction of the surface segment employed in the numerics to one-half of it, using the midplane between the two walls as an additional plane of symmetry, enhances the stability of the bridges if the ratio L_1/L_1 is larger than approximately $L_1/L_1 \approx 2.5$. In this case, the elimination of the modes which are asymmetric with respect to the midplane between the walls leads to stable bridges in a wider region of the parameters. Thus, the symmetry with respect to the midplane between the walls cannot be used in the numerical minimization to further reduce the size of the system.

IV. Different Liquid Morphologies in the Slit Pore

A. Bridges. Bridges are those states in which the liquid connects both walls. We will speak of *extended* bridges when the section of the liquid–vapor interface by the midplane between the walls has a lateral extension which is of the order of L_2 , see Figures 3c,d and 4c,d. These bridges have their contact line *attached* to the $\gamma\delta$ domain boundaries, or, for larger volumes, the contact line detaches and the bridges move onto the lyophobic surface with contact angle θ_δ . In contrast to the extended bridges, for an *anvil-like* bridge the lateral extension of the midplane section is small compared to L_2 , see Figures 3a,b and 4a,b. Typically, an anvil-like bridge extends along the two stripes forming flat channels or *sleeves*, see Figure 1. In the lattice gas model, the particles have finite size and the sleeves of an anvil-like bridge cannot be flatter than the size of the particles. The length of the sleeves along the stripes will depend on the size of the particles,

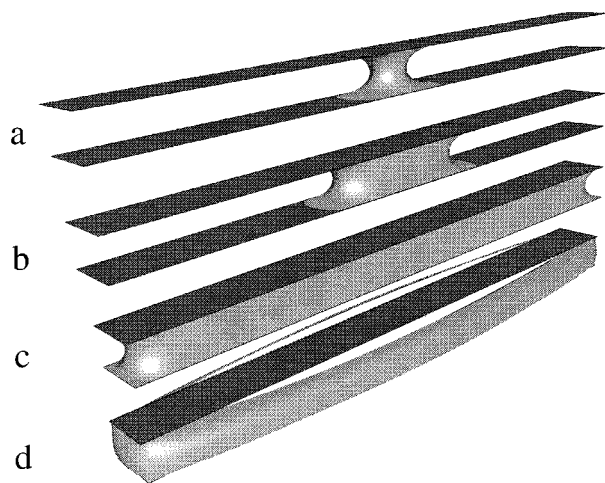


Figure 3. Bridges as obtained by minimization of the effective interface model for slab geometry with fixed ratios $L_1/L_1 = 0.8$ and $L_2/L_1 = 12$. L_\perp , L_1 , and L_2 denote the wall separation, the stripe width, and the length, respectively. The liquid volume V increases from top to bottom: (a) $V = 0.5L_1^3$, (b) $V = 2L_1^3$, (c) $V = 9L_1^3$, and (d) $V = 18L_1^3$.

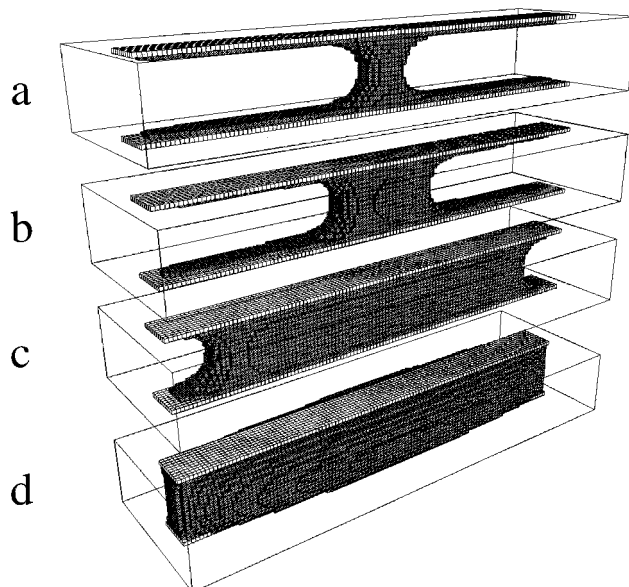


Figure 4. Bridges as obtained from the lattice gas simulations. The position of the interfaces corresponds to average local density $\rho = 0.5$. The slab geometry is characterized by fixed ratios $L_1/L_1 = 1.6$ and $L_2/L_1 = 12$, where the lengths L_\perp , L_1 , and L_2 are as in Figure 3. L_1 is 10 lattice units. The number of particles in the simulation box is (a) $N = 4L_1^3$, (b) $N = 6.4L_1^3$, (c) $N = 18.6L_1^3$, and (d) $N = 37.3L_1^3$. White cubes represent the lyophilic stripes.

the contact angle θ_γ of the liquid with the lyophilic surfaces, and the mean curvature of the liquid–vapor interface. In both the effective interface model and the lattice gas, we choose an interaction between the liquid and the lyophilic stripes that corresponds to $\theta_\gamma = 0$. At large distances from the body of the bridge, the shape of the sleeves approaches the shape of channels with almost translationally invariant cross section. A channel with constant cross section has necessarily positive mean curvature, which implies that an anvil-like bridge with negative mean curvature cannot have arbitrarily long sleeves.

For wall separations $L_1/L_1 < 1$, where l_1 is a characteristic length that is close to L_1 but depends on L_2 , and at sufficiently low volumes of liquid, one can observe anvil-like bridges which are *freely mobile*, that is, bridges with

(25) Meseger, J.; Slobozhanin, L. A.; Perales, J. M. A review on the stability of liquid bridges. *Adv. Space Res.* **1995**, *16*, 5–14.

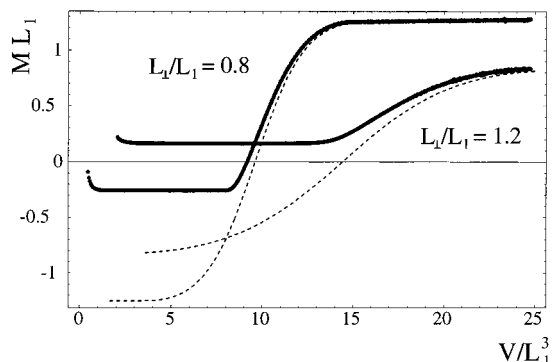


Figure 5. Mean curvature M of the liquid bridges as a function of the liquid volume, for different ratios L_2/L_1 . The thick lines are obtained from numerical minimization of the three-dimensional interface model. The dashed lines represent the mean curvature in the effectively two-dimensional problem with periodic boundary conditions along the stripes and bridges with uniform cross section.

contact lines completely detached from the ends of the lyophilic stripes. Because the liquid phase has no contact to the ends of the stripes, a displacement of these bridges does not cost any energy, see Figure 3a,b. For this kind of bridge, the mean curvature as a function of the volume remains nearly constant and negative in a wide range of volumes, forming a plateau region in Figure 5. Bridges which are formed for ratios $L_2/L_1 > 1$ also exhibit at low volumes a plateau region in the mean curvature, but this time the value of the mean curvature is positive in the plateau, see Figure 5. In the continuous model, the positive mean curvature requires the complete coverage of the stripes by the liquid phase. Hence, the body of the bridge will be connected to *sleeves* that extend to the ends of the lyophilic stripes, see Figure 1. An anvil-like liquid bridge with sleeves that cover the full length of the stripes “feels” a force that tends to keep it in the middle of the stripes. For small volumes, the body of the bridge is rather slim as shown in Figures 3a and 4a. When one starts from such a bridge and increases the liquid volume V , the body of the bridge is extended parallel to the lyophilic stripes while its mean curvature M remains unchanged, see the plateau region in Figure 5.

It is instructive to compare our results with those from previous studies^{4–6} that assumed the cross section of the liquid morphologies (bridges and channels) to be always translationally invariant along the stripes. In ref 6, an effectively two-dimensional interface model representing the cross section of the pore is used to determine the equilibrium morphologies. In Figure 5, the dashed lines correspond to the mean curvature M as obtained from this two-dimensional model (multiplying the volume per unit length by L_2). For small V , the typical morphologies in the three-dimensional model are anvil-like bridges (Figure 1) that have a similar mean curvature for different volumes leading to the plateau region in Figure 5. Such bridges cannot occur in the two-dimensional constant cross section model. For larger values of V , the bridges obtained using the three-dimensional model have almost constant two-dimensional cross-section, see Figures 3c and 4c. For even larger volumes of liquid, the contact line detaches from the $\gamma\delta$ boundary, and the bridges bulge outward, see Figures 3d and 4d.

B. Channels and Bulged Channels. The morphology of wetting layers on a lyophobic substrate with a single lyophilic stripe has been studied before.^{2,3} One starts with a completely dewetted stripe of finite length and slowly deposits a certain volume V of liquid on it. For small V ,

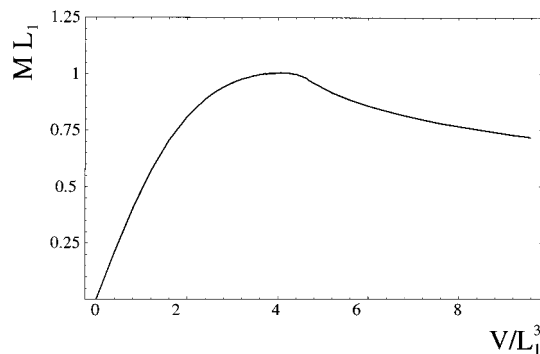


Figure 6. Mean curvature M of the channel on a single stripe as a function of the rescaled volume V/L_1^3 , for $L_2/L_1 = 12$.

the liquid forms a channel that has almost uniform cross section along the stripe. This means that for small V the channel has a shape similar to a cylindrical segment, with the contact line attached to the $\gamma\delta$ boundaries of the stripe. If V is increased, the channel grows, keeping its cross section almost constant along the stripe (*homogeneous channel*). When the channel reaches a volume per unit length close to $(\pi/8)L_1^2$, where L_1 is the width of the stripe, it undergoes a transition to a state with a cross section that changes strongly when we move along the stripe. In this state, the largest part of the volume is concentrated in a “bulge” that extends into the stripe forming flat sleeves similar to the sleeves of an anvil-like bridge in the slit pore. However, for a bulge on a single stripe, the contact line cannot detach from the $\gamma\delta$ domain boundary (if the contact angle within the stripe is zero and the finite size of the particles is not taken into account), because the bulge has positive mean curvature for every volume.

For a long single stripe with $L_2/L_1 \gtrsim 18$, the morphological transition between a homogeneous channel and a channel with a single bulge is discontinuous, see ref 2. In contrast, a single stripe of length $L_2/L_1 \lesssim 18$ exhibits not a first order but a continuous transition at a certain characteristic volume of liquid. In this case, the mean curvature, M , of the stable states as a function of the volume has only one branch, see Figure 6. For all ratios L_2/L_1 , two different stationary morphologies exist for a given mean curvature, M , one at small volume (channel) and the other at large volume (bulge).

Let us go back to the slit pore and discuss the behavior of the broken bridges, that is, of the shapes with two disconnected volumes. We allow the two bodies of liquid to exchange volume with each other. It is clear that the stable shapes of the volume of liquid on each one of the stripes are minimizers of the functional in (11) with respect to the volume constraint in (12) for the portion of volume gained in stable equilibrium with the liquid on the other stripe. If we couple two stable systems having the same mean curvature, the resulting system does not need to be stable. Nonetheless, all stable configurations for a system consisting of two identical subsystems can be constructed if the stable states of a single subsystem are known for all volumes.

For the slit pore, different morphologies are expected for different volumes, see Figure 7, if the volume of liquid is not sufficient to bridge the walls. At low volumes, both stripes are covered by a channel of almost constant cross section. To fulfill the Laplace equation, both constant cross section channels must have the same mean curvature and, thus, the same volume (symmetric configuration). At large volumes of liquid, one of the stripes is covered by a channel with a bulge and the other is covered by a channel with a cross section similar to the cross section of the sleeves

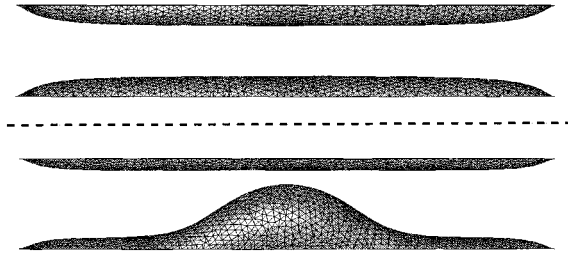


Figure 7. Disconnected channels as obtained within the effective interface model: (top) symmetric configuration for rescaled volume $V/L_1^3 = 7$ and (bottom) asymmetric configuration for $V/L_1^3 = 9$, for the ratios $L_1/L_1 = 2$ and $L_2/L_1 = 12$.

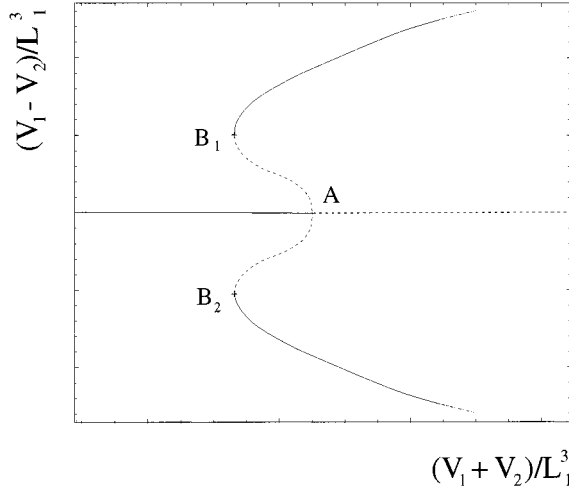


Figure 8. Schematic diagram for the bifurcation of the difference in volume, $V_1 - V_2$, between two volumes of liquid on identical stripes as a function of the total volume, $V_1 + V_2$. The symmetric branch beyond A, at $V_1 - V_2 = 0$, and the branches AB_1 and AB_2 refer to unstable configurations (dashed lines).

that extend from the bulge on the first stripe. In the case of a bulge coexisting with a homogeneous channel, the volume of the channel with the bulge can be much larger than the volume of the other channel (asymmetric configuration). Notice that because of the positive mean curvature of all broken configurations, both stripes are completely covered if the contact angle is zero within the lyophilic domains.

When two bodies of liquid on two identical stripes of length $L_2/L_1 = 12$ are considered, the stationarity condition demands that the mean curvature has to be the same and positive for both bodies. The analysis for the single stripe as discussed at the beginning of this section implies that there are two stationary morphologies for a given mean curvature. For two stripes, analogous arguments lead to a bifurcation from one symmetric to two asymmetric and one symmetric stationary configurations as the total volume is increased, see Figure 8. The two asymmetric configurations correspond to a homogeneous channel on one stripe and a bulged channel on the other and are stable for large V . For small V , a symmetric configuration with two channels of almost constant and identical cross section is stable, whereas for large V , the symmetric configuration consisting of two bulges is unstable. Notice that although the transition is continuous for a single stripe of length $L_2/L_1 = 12$, it is of first order when one considers two identical stripes of this length in equilibrium. Here, we assumed the stripes to be sufficiently far apart so that the two liquid surfaces cannot intersect. In the slit pore, these broken morphologies are in competition with the bridges studied in the former section. A similar symmetry breaking

at increasing volumes has been found by Lenz and Lipowsky¹ for two identical circular lyophilic domains, with the difference that in that case the transition is continuous.

V. Chemical Potential versus Pressure Difference

At equilibrium, the chemical potential must be the same in the two coexisting phases, but the pressure will be the same in both phases only if they are separated by a flat interface, as required by the Laplace equation. Let us consider the connection between the chemical potential and the pressure difference across the liquid–vapor interface, ΔP .²⁶ At constant temperature, in each one of the phases the chemical potential, μ , the pressure, P , and the density, ρ , are related by the equations

$$\frac{\partial \mu_\alpha}{\partial P}|_{T, P_\alpha} = \frac{1}{\rho_\alpha} \quad \text{and} \quad \frac{\partial \mu_\beta}{\partial P}|_{T, P_\beta} = \frac{1}{\rho_\beta} \quad (15)$$

By P_0 , we denote the saturated vapor pressure, which is the coexistence pressure of the liquid at equilibrium with its vapor across a planar interface. ρ_α^0 and ρ_β^0 denote the density of the α and β phase, respectively, in this state. Assuming that the β phase (liquid) is incompressible, we integrate eq 15 for this phase from P_0 to P_β ,

$$\mu_\beta(T, P_\beta) - \mu_\beta(T, P_0) = \frac{1}{\rho_\beta^0}(P_\beta - P_0) \quad (16)$$

Starting from the equality of the chemical potential in both phases at equilibrium,

$$\mu_\beta(T, P_\beta) = \mu_\alpha(T, P_\alpha) \quad (17)$$

we expand the chemical potential in the α and in the β phase to first order in terms of $(P_\alpha - P_0)$ and $(P_\beta - P_0)$, respectively, and use (15), which leads to

$$P_\beta - P_0 \approx \frac{\rho_\beta^0}{\rho_\alpha^0 - \rho_\beta^0}(P_\alpha - P_\beta) \quad (18)$$

Substituting (16) and $\Delta P \equiv P_\alpha - P_\beta$, the last equation becomes

$$\mu_\beta(T, P_\beta) - \mu_\beta(T, P_0) \approx \frac{\Delta P}{\rho_\alpha^0 - \rho_\beta^0} \quad (19)$$

Thus, the difference in chemical potential between the curved and the planar interface and the pressure difference across the curved interface, ΔP , are proportional to each other with a proportionality constant $1/(\rho_\alpha^0 - \rho_\beta^0)$. Because ΔP is proportional to M , according to the Laplace equation (13), $\mu \sim M$ apart from an additive constant.

In Figure 9, we plot the chemical potential μ for bridges in the lattice gas as a function of the number of particles N in the box. In Figure 5, we plot the mean curvature M against the volume V obtained from the numerical minimization of the effective interface model. In both cases, we start from large V and decrease it until the bridge breaks. Figures 9 and 5 are very similar, because, as we have shown, μ is linearly related to the mean curvature. For a wide range of wall separations L_\perp , two plateau regions are observed for the functional dependence of M

(26) Rowlinson, J. S.; Widom, B. *Molecular theory of capillarity*; Oxford University Press: New York, 1989.

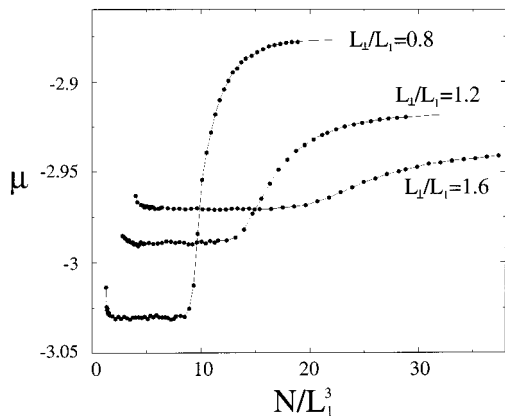


Figure 9. Chemical potential μ in the lattice gas simulations as a function of the number of particles N , for different values of the ratio L_2/L_1 . The width of the stripes, L_1 , is 10 lattice units.

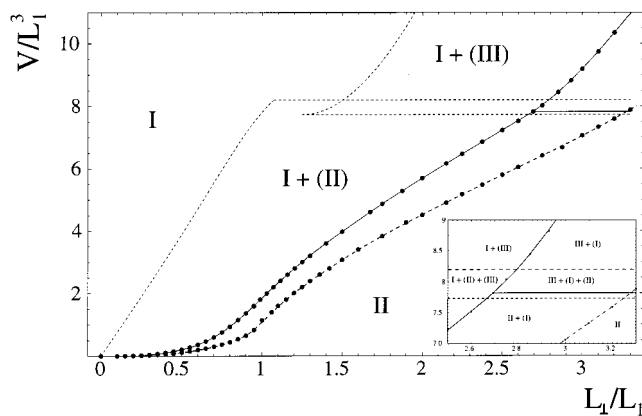


Figure 10. Shape diagram for the slit pore with $L_2/L_1 = 12$ as a function of the rescaled volume V and the rescaled wall separation L_1 . The different morphologies of the channels and the bridges in regimes I, II, and III are explained in section VI. The coexistence curves and the metastability limits (or spinodals) correspond to the full and dashed lines, respectively.

on V and the dependence of μ on N . The plateau region at large V corresponds to bridges that detach from the boundaries of the stripes, bulging outward onto the lyophobic domains, see Figures 3d and 4d. The mean curvatures of these bridges have similar values, decreasing slightly with decreasing V . At a certain volume, the contact line attaches to the boundaries of the stripes and the cross section of the bridges becomes almost invariant along the stripes, see Figures 3c and 4c. If V is decreased further, M decreases quickly, until the plateau region at low V is reached. In this plateau region, the body of the bridge shrinks in length with decreasing V and forms an anvil-like bridge, see Figures 3b and 4b. The mean curvature of such an anvil-like bridge is almost constant within the plateau region at low V . For even smaller values of V , the mean curvature increases with decreasing V , as is expected for a bridge that is close to rupture, see Figures 4a and 3a.

VI. Shape or “Phase” Diagram

Because the contact angles on the lyophilic and lyophobic domains are $\theta_\gamma = 0$ and $\theta_\delta = \pi$, respectively, and the ratio $L_2/L_1 = 12$, the only parameters still adjustable are the volume V and the ratio L_1/L_1 of the wall separation to the stripe width.

The shape or “phase” diagram shown in Figure 10 has been obtained from numerical minimization of the inter-

face model and specifies the regions where certain interfacial shapes (configurations) are either *global* minima of the free energy in (10) for a given value of V or only *local* minima. The boundaries of the latter regions are analogous to spinodal lines. Configurations are denoted by Roman numbers which appear in the regions of the shape diagram where these configurations are local or global minima. We use brackets to indicate metastable states corresponding to local minima.

For small ratios L_1/L_1 , we find the bridges (labeled by I) to have the lowest free energy. For larger values of L_1/L_1 , disconnected configurations with two channels are more favorable. These can be symmetric (two identical channels) or asymmetric (one channel and one bulged channel) and are labeled by II and III, respectively. We find a triple point for the bridges, I, and the two-channel configurations, II and III, at the ratio $L_1/L_1 \approx 2.70$ and the reduced volume $V/L_1^3 \approx 7.82$. Two qualitatively different mechanisms lead to destabilization of the disconnected configurations II and III: (i) The exchange of liquid between the two channels is included in the model as part of the equilibrium conditions and, thus, is effective for any value of L_1 . Such an instability gives rise to horizontal “spinodals” in the shape diagram of Figure 10; (ii) If the two channels touch each other, a bridge must be formed. This latter mechanism depends on L_1 . The stability limit of the bridges was detected by changing L_1 or V in small steps and minimizing the interfacial free energy after each step. We estimate the relative error in the values at which the interfacial shape becomes unstable to be less than 2% for runs with constant L_1 . The relative error in the distance of rupture is also smaller than 2% for runs with constant V and increasing L_1 . To obtain these estimates, we performed a series of runs using different interface discretizations, that is, different size distributions of the triangles forming the surface, and varied the step sizes of the control parameter L_1 or V .

VII. Summary and Outlook

In summary, we have studied the morphology of liquid phases within chemically structured slit pores. For striped surface domains, both the lattice gas models and the effective interface models lead to liquid bridges which have an anvil-like shape for a wide range of parameter values. We also determined additional liquid morphologies consisting of two disconnected channels, as discussed in section IV.B. Another subtle aspect of our study is the position of the contact line which can detach from the boundary of the γ domain even for contact angle $\theta_\gamma = 0$ provided the $(\alpha\beta)$ interface has negative mean curvature, see sections III.B. and IV.A. To be specific, we have chosen the terminology which is appropriate for a system close to liquid–vapor coexistence. However, our results apply equally well to two-phase coexistence in multicomponent liquids for which the α and β phases are two different liquids.

For simplicity, we have focused here on the simplest geometry of the surface domains. Additional geometries have been studied in ref 6 for bridges and channels with constant cross section. These geometries include (i) relative shifts of the two opposing stripes which act to shear and, thus, to break the bridges and (ii) many parallel stripes on both surfaces which lead to a whole cascade of morphological wetting transitions. Likewise, one may study the evolution of the wetting morphologies as one tilts or rotates one surface with respect to the other. In all of these cases, anvil-like bridges will again be present for a wide range of parameter values.

Acknowledgment. Support by the Deutsche Forschungsgemeinschaft via the Sonderforschungsbereich 488 and via the Schwerpunktprogramm on wetting is gratefully acknowledged.

Appendix

To show the desired inequality $M \leq 0$, we choose a point \mathbf{x}_0 of the contact line, $\angle_{\alpha\beta\sigma}$, lying in the interior of a γ domain with $\theta_\gamma = 0$. A small part of the contact line around \mathbf{x}_0 which is also located in the interior of the γ domain is parametrized by a curve $\mathbf{r}_1(t)$ where t is the arc length of the curve with $-|t_a| < t < |t_b|$ and $\mathbf{r}_1(0) = \mathbf{x}_0$. Because we assume the contact line to be smooth in the interior of the γ domain, the tangent $\mathbf{t}_1(t)$ and the curvature vector $\mathbf{k}_1(t)$ of this curve are defined for all t by

$$\mathbf{t}_1(t) = \frac{d}{dt}\mathbf{r}_1(t) \text{ and } \mathbf{k}_1(t) = \frac{d^2}{dt^2}\mathbf{r}_1(t)$$

The contact line lies within the plane of the wall, which implies that the tangent $\mathbf{t}_1(t)$ and the curvature vector $\mathbf{k}_1(t)$ lie in the plane of the wall as well. From the theorem of Meusnier, the normal curvature $c_1(\mathbf{x}_0)$ of the liquid surface in the direction tangential to the contact line at the point \mathbf{x}_0 is

$$c_1(\mathbf{x}_0) = -\mathbf{k}_1(0) \cdot \hat{\mathbf{N}}_{\alpha\beta}(\mathbf{x}_0)$$

with $\hat{\mathbf{N}}_{\alpha\beta}(\mathbf{x}_0)$ being the unit vector normal to the $\alpha\beta$ interface at the point \mathbf{x}_0 , see for instance ref 27. Because the contact angle θ_γ is equal to zero on the γ domain, the vector normal to the wall, $\hat{\mathbf{N}}_\sigma$, must be parallel to $\hat{\mathbf{N}}_{\alpha\beta}(\mathbf{x}_0)$, which implies that $c_1(\mathbf{x}_0)$ has to be zero.

Let us now consider a cut through the surface of the liquid by a plane perpendicular to the tangent vector $\mathbf{t}_1(0)$ at \mathbf{x}_0 . The contour of the intersection between the liquid surface and the plane close to the point \mathbf{x}_0 can be parametrized by a smooth curve $\mathbf{r}_2(t')$, with t' being the arc length, $0 \leq t' < \eta$ with $\eta > 0$, and $\mathbf{r}_2(0) = \mathbf{x}_0$. By the condition that the contact angle θ_γ is equal to zero in \mathbf{x}_0 , the tangent vector at the point \mathbf{x}_0 , $\mathbf{t}_2(0)$, has to lie within the plane of the wall. Because the curve $\mathbf{r}_2(t')$ stays above the planar wall, the curvature vector $\mathbf{k}_2(0)$ of this curve at \mathbf{x}_0 has to point toward the half-space above the planar wall.

Because $\hat{\mathbf{N}}_{\alpha\beta}$ and $\hat{\mathbf{N}}_\sigma$ coincide at \mathbf{x}_0 for $\theta_\gamma = 0$, we find the normal curvature of the $\alpha\beta$ interface at \mathbf{x}_0 in the direction perpendicular to the contact line, $c_2(\mathbf{x}_0)$, to be

$$c_2(\mathbf{x}_0) = -\mathbf{k}_2(0) \cdot \hat{\mathbf{N}}_{\alpha\beta}(\mathbf{x}_0) \leq 0$$

Because the intersecting planes are perpendicular to each other, the mean curvature M satisfies

$$M = \frac{1}{2}(c_1(\mathbf{x}_0) + c_2(\mathbf{x}_0)) \leq 0$$

List of Symbols

α	vapor phase
β	liquid phase
γ	lyophilic substrate

δ	lyophobic substrate
ΔP	pressure difference between the vapor and liquid phase
ϵ	coupling constant between particles in lattice gas
ϵ_γ	coupling constant between particles and lyophilic surface domains
ϵ_δ	coupling constant between particles and lyophobic surface domains
η	positive real number
Λ_T	thermal wavelength
θ	contact angle
μ	chemical potential
μ_0	chemical potential at bulk coexistence
μ_{fluid}	chemical potential of the classical fluid
ρ	particle number density
Σ	interfacial energy
σ	substrate surfaces or walls of the slit pore
Ω_1	set of lattice cells adjacent to the walls
\mathcal{A}	surface
$ \mathcal{A} $	area of the surface \mathcal{A}
a	lattice spacing in lattice gas
c	normal curvature of the liquid surface
\mathcal{F}	free energy of all interfaces
$\hat{\mathcal{F}}$	free energy in the constant pressure ensemble
f	frequency of a single cell configuration
H	surface field in Ising model
\mathcal{H}	Hamiltonian of Ising model
\mathcal{H}_{LG}	Hamiltonian of lattice gas
I	interval of real numbers
J	coupling constant between spins in Ising model
\mathbf{k}	curvature vector
k_B	Boltzmann constant
$\angle_{\alpha\beta\sigma}$	three phase contact line
L_1	width of the γ stripes
L_2	length of the γ stripes
L_\perp	wall separation
\underline{L}	characteristic distance between the walls
\mathcal{M}	total magnetization in Ising model
M	mean curvature
m	magnetization per spin in Ising model
m_p	mass of a particle in the classical fluid
\mathcal{N}	number of cells in lattice model
N	number of particles in lattice gas
n	occupation number in lattice gas, $n = 0$ or 1
$\hat{\mathbf{N}}_{\alpha\beta}$	normal to the liquid surface
$\hat{\mathbf{N}}_\sigma$	normal to the substrate
P	pressure
$\mathbf{r}(t)$	parametrization of a curve
\mathcal{S}_m	local state around a particular lattice cell
s	spin variable in Ising model, $s = -1$ or $+1$
T	temperature
\mathbf{t}	tangent vector of a curve
t	arc length of a curve
\mathcal{V}	spatial region
$ \mathcal{V} $	volume of the spatial region \mathcal{V}
V	volume of liquid phase
\mathbf{x}_0	point on the contact line

(27) do Carmo, M. P. *Differential Geometry of Curves and Surfaces*; Prentice Hall: Englewood Cliffs, NJ, 1976.